

Tripartite entanglement and matrix inversion quantum algorithm

Mi-Ra Hwang¹, MuSeong Kim¹, Eylee Jung¹, Chang-Yong Woo¹, and DaeKil Park^{1,2*}

¹*Department of Electronic Engineering,*

Kyungnam University, Changwon 631-701, Korea

²*Department of Physics, Kyungnam University, Changwon 631-701, Korea*

Abstract

The role of entanglement is discussed in the Harrow-Hassidim-Lloyd (HHL) algorithm. We compute all tripartite entanglement at every steps of the HHL algorithm. The tripartite entanglement is generated in the first quantum phase estimation (QPE) step. However, it turns out that amount of the generated entanglement is not maximal except very rare cases. In the second rotation step some tripartite entanglement is annihilated. Thus, the net tripartite entanglement is diminished. At the final inverse-QPE step the matrix inversion task is completed at the price of complete annihilation of the entanglement. An implication of this result is discussed.

* dkpark@kyungnam.ac.kr

I. INTRODUCTION

In quantum information processing quantum entanglement[1–3] plays an important role as a physical resource. It is used in various quantum information processing, such as quantum teleportation[4, 5], superdense coding[6], quantum cloning[7], quantum cryptography[8, 9], quantum metrology[10], and quantum computer[11–13]. Furthermore, quantum computers with hundred qubits were already constructed in IBM and Google. In this reason the development of quantum algorithms becomes important more and more to use the quantum computers efficiently.

The representative of the quantum algorithm are Shor’ factoring[14] and Grover’s search[15] algorithms. Few years ago another quantum algorithm[16] called Harrow-Hassidim-Lloyd (HHL) algorithm was developed. It is a quantum algorithm, which can compute the inverse of sparse matrix. If A is a $N \times N$ sparse matrix, HHL algorithm completes the inversion task with a runtime of $\mathcal{O}(s^2\kappa^2 \log(N)/\epsilon)$, where s is the maximum number of non-zero entries in row or column, κ the condition number, and ϵ the precision. Since same task can be implemented in the classical computer with a runtime of $\mathcal{O}(s\kappa N \log(1/\epsilon))$ even though the most efficient algorithm is adopted, one can say that the HHL algorithm improves exponentially in the matrix inversion task over the best classical algorithm. This algorithm is based on the efficient Hamiltonian simulation[17]. Subsequently, there was a proposals to deal with dense matrices[18]. Also a hybrid algorithm[19] was proposed, where both classical and quantum computers are used appropriately.

In this paper we examine a question: ‘how much the HHL algorithm uses the quantum entanglement efficiently?’. In order to explore this issue we compute the tripartite entanglement in every steps of the HHL algorithm by choosing an experimental realization of the algorithm presented in Ref. [20]. Since the HHL algorithm is known to be optimal[16] in the matrix inversion task and entanglement is known as a physical resource, we expect that much entanglement is created and finally annihilated during the process of the algorithm. However, it turns out that maximal tripartite entanglement is not created except very rare cases. As expected, all created entanglement is annihilated at the final step of the algorithm.

This paper is organized as follows. In Sec. II we discuss the role of entanglement in the Grover’s algorithm. In Sec. III we compute the three-tangle[21] of some rank-2 mixture. The result of this section will be used in Sec. V. In Sec. IV we briefly review the HHL

algorithm. In Sec. V we compute the tripartite entanglement at every steps of the HHL algorithm. In Sec. VI a conclusion and further discussion are presented. In appendix A the quantum phase estimation (QPE) is discussed when the unitary operator U is operated to the non-eigenvector $|\psi\rangle$. The result of this appendix is used in Sec. IV.

II. ENTANGLEMENT IN GROVER'S ALGORITHM

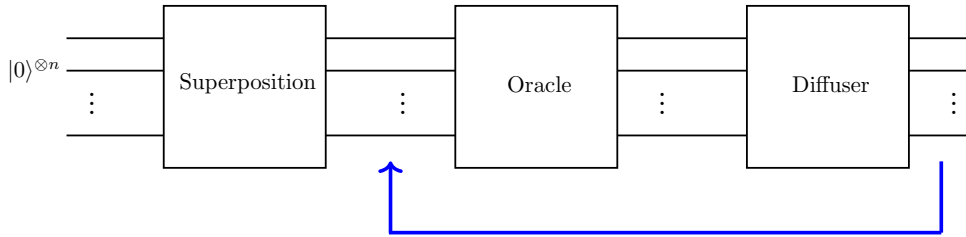


FIG. 1: (Color online) The schematic representation of the Grover's algorithm. The oracle and diffuser unitary transformations should be repeated roughly \sqrt{N} times for large N .

Let us consider a set $\mathcal{S} = \{|j\rangle | j = 0, 1, \dots, N-1\}$ with $\langle j_1 | j_2 \rangle = \delta_{j_1 j_2}$. Grover's algorithm[15, 22] is a quantum algorithm, which tries to find a particular quantum state $|\psi_G\rangle \in \mathcal{S}$. Grover's algorithm consists of three unitary transformations called superposition, oracle, and diffuser. The superposition transforms the initial state $|0\rangle^{\otimes n}$ to a superposed state, where all states in \mathcal{S} are superposed with equal probability amplitude. This can be achieved by making use of the Hadamard gate

$$H = \frac{1}{\sqrt{2}} \begin{pmatrix} 1 & 1 \\ 1 & -1 \end{pmatrix}. \quad (2.1)$$

Therefore, after superposition transformation the initial state is changed into

$$|s\rangle = H^{\otimes n} |0\rangle^{\otimes n} = \frac{1}{\sqrt{N}} \sum_{j=0}^{N-1} |j\rangle \quad (2.2)$$

where $N = 2^n$. The oracle and diffuser are described by the unitary operators $U_{\text{oracle}} = \mathbb{1} - 2|\psi_G\rangle\langle\psi_G|$ and $U_{\text{diffuser}} = 2|s\rangle\langle s| - \mathbb{1}$, respectively. The oracle changes a sign of $|\psi_G\rangle$ in $|s\rangle$. The diffuser increases the probability amplitude of $|\psi_G\rangle$ from $U_{\text{oracle}}|s\rangle$. Given N the oracle and diffuser transformations are repeated roughly \sqrt{N} times[23–25]¹ for large N . The schematic quantum circuit of the Grover’s algorithm is plotted in Fig. 1.

The role of entanglement manifestly appears when $N = 4$. If we assume $|\psi_G\rangle = |3\rangle = |11\rangle$ in this case, U_{oracle} transforms $|s\rangle$ into

$$|\psi_{\text{oracle}}\rangle = U_{\text{oracle}}|s\rangle = \frac{1}{2}(|00\rangle + |01\rangle + |10\rangle - |11\rangle). \quad (2.3)$$

Since the concurrence, one of the bipartite entanglement measure, is defined as $\mathcal{C} = 2|a_{00}a_{11} - a_{01}a_{10}|$ for two qubit pure state $|\psi\rangle = \sum_{i,j=0}^1 a_{ij}|ij\rangle$ [26, 27], U_{oracle} changes the separable state $|s\rangle$ into the maximally entangled state $|\psi_{\text{oracle}}\rangle$. Then, U_{diffuser} exactly detects $|\psi_G\rangle$, which means $U_{\text{diffuser}}|\psi_{\text{oracle}}\rangle = |\psi_G\rangle$. Therefore, U_{oracle} creates an entanglement maximally and U_{diffuser} increases the probability amplitude of $|\psi_G\rangle$ maximally at the price of complete annihilation of entanglement.

	$ \psi_1\rangle$	$ \psi_2\rangle$	$ \psi_3\rangle$	$ \psi_4\rangle$
τ_3	1/4	1/16	9/64	9/256
\mathcal{C}_{AB}	1/2	1/4	3/8	3/16
\mathcal{C}_{AC}	1/2	1/4	3/8	3/16
\mathcal{C}_{BC}	1/2	1/4	3/8	3/16

Table I: Entanglement flow in Grover’s algorithm when $N = 8$

Even though Grover’s algorithm is optimal as a quantum searching algorithm[28], such maximal creation and complete annihilation of entanglement do not occur for large N . For example, let us consider $N = 8$ case. If $|\psi_G\rangle = |7\rangle = |111\rangle$, Grover’s algorithm changes the

¹ As proved in Ref. [25], the optimal number of queries is $\pi\sqrt{N}/4$ when N is very large.

quantum state as

$$\begin{aligned}
|\psi_1\rangle &= U_{\text{oracle}}|s\rangle = \frac{1}{2\sqrt{2}}(|0\rangle + |1\rangle + |2\rangle + |3\rangle + |4\rangle + |5\rangle + |6\rangle - |7\rangle) \\
|\psi_2\rangle &= U_{\text{diffuser}}|\psi_1\rangle = \frac{1}{4\sqrt{2}}(|0\rangle + |1\rangle + |2\rangle + |3\rangle + |4\rangle + |5\rangle + |6\rangle + 5|7\rangle) \\
|\psi_3\rangle &= U_{\text{oracle}}|\psi_2\rangle = \frac{1}{4\sqrt{2}}(|0\rangle + |1\rangle + |2\rangle + |3\rangle + |4\rangle + |5\rangle + |6\rangle - 5|7\rangle) \\
|\psi_4\rangle &= U_{\text{diffuser}}|\psi_3\rangle = -\frac{1}{8\sqrt{2}}(|0\rangle + |1\rangle + |2\rangle + |3\rangle + |4\rangle + |5\rangle + |6\rangle - 11|7\rangle).
\end{aligned} \tag{2.4}$$

The three-tangles τ_3 [21] for $|\psi_i\rangle$ and concurrences[26, 27] for the reduced mixed states are summarized in Table I. As Table I shows, U_{oracle} transforms the separable state $|s\rangle$ to $|\psi_1\rangle$, whose three-tangle is $1/4$. Since maximum three-tangle is 1^2 , $|\psi_1\rangle$ is only partially entangled state. Thus, maximal entanglement creation does not occur in this case. U_{diffuser} changes $|\psi_1\rangle$ into $|\psi_2\rangle$, whose three-tangle is $1/16$. Therefore, the complete annihilation of tripartite entanglement also does not occur. Same is true for $|\psi_3\rangle$ and $|\psi_4\rangle$. Similar behavior occurs in the bipartite entanglement.

III. THREE-TANGLE FOR RANK-2 MIXED STATE ρ

In this section we compute the three-tangle of following rank-2 mixed state ρ for later use. The state is given by

$$\rho = p|\phi_1\rangle\langle\phi_1| + (1-p)|\phi_2\rangle\langle\phi_2| \tag{3.1}$$

where $0 \leq p \leq 1$ and

$$\begin{aligned}
|\phi_1\rangle &= \frac{x_1}{\sqrt{2}}(|010\rangle - |011\rangle) + \frac{x_2}{\sqrt{2}}(|100\rangle + |101\rangle) \\
|\phi_2\rangle &= -\frac{x_2}{\sqrt{2}}(|010\rangle - |011\rangle) + \frac{x_1}{\sqrt{2}}(|100\rangle + |101\rangle)
\end{aligned} \tag{3.2}$$

with $0 \leq x_1 \leq 1$ and $x_2 = \sqrt{1 - x_1^2} \geq 0$. It is straightforward to show that the three-tangles of $|\phi_1\rangle$ and $|\phi_2\rangle$ are the same as $4x_1^2x_2^2$. Therefore, the three-tangle of ρ should satisfy

$$\tau_3(\rho) = 4x_1^2x_2^2 \quad \text{when } p = 0 \text{ or } p = 1. \tag{3.3}$$

² Maximal three-tangle is realized in the Greenberger-Horne-Zeilinger (GHZ) state[29]

$$|GHZ\rangle = \frac{1}{\sqrt{2}}(|000\rangle + |111\rangle)$$

and its local unitary transformed states.

For mixed states the three-tangle is defined by a convex-roof method[30, 31] as follows:

$$\tau_{ABC}(\rho) = \min_i \sum p_i \tau_{ABC}(\rho_i), \quad (3.4)$$

where the minimum is taken over all possible ensembles of pure states. The pure state ensemble corresponding to the minimum τ_{ABC} is called optimal decomposition. It is in general difficult to derive the optimal decomposition for arbitrary mixed states. The three-tangle for nontrivial rank-2 mixed state was explicitly computed in [32]. In Ref. [33] it was shown that the three-tangle can be computed by constructing the convex hull in the minimum of characteristic curves. Using such a method the three-tangles for higher-rank mixed states were computed[34, 35].

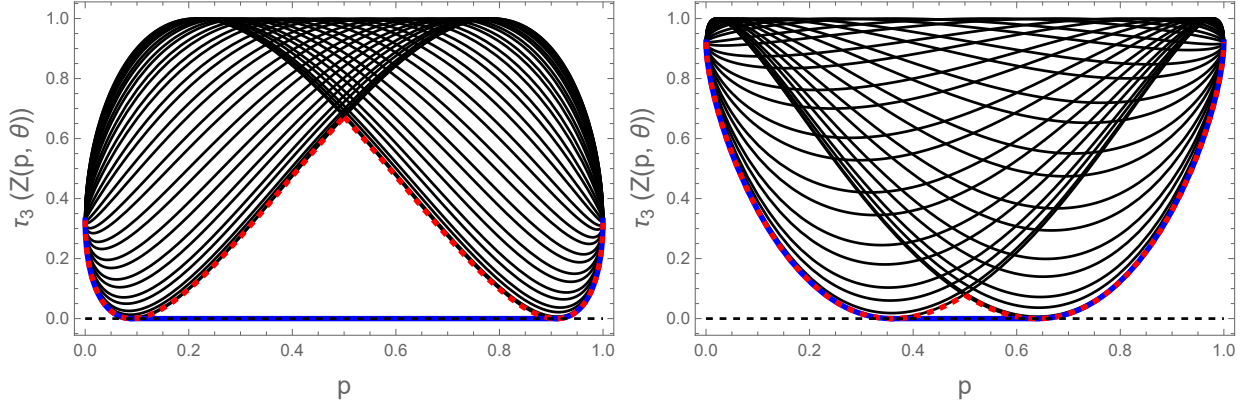


FIG. 2: (Color online) Characteristic curves at (a) $x_1 = 0.3$ and (b) $x_1 = 0.8$. Minimum of the curves is plotted as a thick dashed (red) curve. The convex hull is plotted as a think blue curve.

In order to compute the three-tangle of ρ for arbitrary p we define

$$|Z(p, \theta)\rangle = \sqrt{p}|\phi_1\rangle - e^{i\theta}\sqrt{1-p}|\phi_2\rangle = y_1(|010\rangle - |011\rangle) + y_2(|100\rangle + |101\rangle) \quad (3.5)$$

where

$$y_1 = \frac{1}{\sqrt{2}} \left[\sqrt{p}x_1 + e^{i\theta}\sqrt{1-p}x_2 \right] \quad y_2 = \frac{1}{\sqrt{2}} \left[\sqrt{p}x_2 - e^{i\theta}\sqrt{1-p}x_1 \right]. \quad (3.6)$$

Then, one can show that the three-tangle for $|Z(p, \theta)\rangle$ is given by

$$\begin{aligned} \tau_3(Z(p, \theta)) &= 16|y_1 y_2|^2 \\ &= 4 \left[\left[p^2 + (1-p)^2 - 2p(1-p)\cos 2\theta \right] x_1^2 x_2^2 \right. \\ &\quad \left. + p(1-p)(x_1^2 - x_2^2)^2 - 2\sqrt{p(1-p)}(2p-1)x_1 x_2 (x_1^2 - x_2^2) \cos \theta \right]. \end{aligned} \quad (3.7)$$

The $\tau_3(Z(p, \theta))$ is plotted in Fig. 2 when (a) $x_1 = 0.3$ and (b) $x_1 = 0.8$ with choosing θ from 0 to 2π as an interval 0.2. Both figures show that $\tau_3(Z(p, \theta))$ is minimized by

$$f(p) = \min \left[\tau_3(Z(p, 0)), \tau_3(Z(p, \pi)) \right]. \quad (3.8)$$

This curve is plotted in Fig. 2 as thick dashed red lines. Fig. 2 also show that $f(p) = 0$ at $p = p_{\pm}$, where

$$p_{\pm} = \frac{1}{2} [1 \pm |x_1^2 - x_2^2|]. \quad (3.9)$$

One can show that $f''(p)$ is negative in some region depending on x_1 and x_2 between p_- and p_+ . Therefore, $\tau_3(\rho)$, the convex hull of $f(p)$, can be written in a form

$$\tau_3(\rho) = \begin{cases} f(p) & p \leq p_- \text{ or } p \geq p_+ \\ 0 & p_- \leq p \leq p_+. \end{cases} \quad (3.10)$$

This is plotted in Fig. 2 as thick blue line.

IV. BRIEF REVIEW OF HHL ALGORITHM

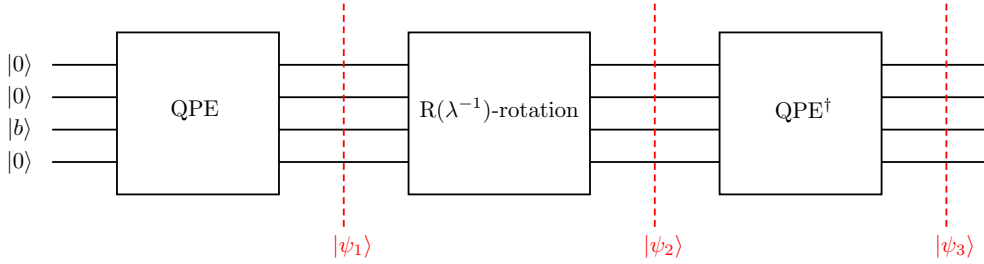


FIG. 3: (Color online) The schematic representation of the HHL algorithm.

The HHL algorithm[16] consists of three steps, which are QPE[36–38], $R(\lambda^{-1})$ -rotation, and inverse QPE. The schematic quantum circuit of the HHL algorithm is plotted in Fig. 3. These three steps were experimentally and explicitly realized in Ref. [20]³ by selecting a

³ In Fig. 1 of Ref. [20] the rotations $R_y(\pi/2^r)$ and $R_y(2\pi/2^r)$ should be interchanged.

linear equation $A\mathbf{x} = \mathbf{b}$, where

$$A = \frac{1}{2} \begin{pmatrix} 3 & 1 \\ 1 & 3 \end{pmatrix} \quad \mathbf{b} = \begin{pmatrix} b_0 \\ b_1 \end{pmatrix} \quad (4.1)$$

where $b_0^2 + b_1^2 = 1$. If A is not hermitian, one can change the linear equation by $\tilde{A}\mathbf{y} = \begin{pmatrix} \mathbf{b} \\ \mathbf{0} \end{pmatrix}$

where \tilde{A} is a hermitian matrix given by $\tilde{A} = \begin{pmatrix} 0 & A \\ A^\dagger & 0 \end{pmatrix}$.

At the QPE stage we perform the QPE-algorithm by applying the unitary operator e^{iAt} to $|b\rangle = b_0|0\rangle + b_1|1\rangle$. As shown in the appendix A, after the QPE stage the quantum state becomes

$$|\psi_1\rangle = \sum_i \beta_i |\lambda_i\rangle |u_i\rangle \otimes |0\rangle \quad (4.2)$$

if one chooses $t = 2\pi/2^n$. In Eq. (4.2) λ_i and $|u_i\rangle$ are the eigenvalue and corresponding eigenvector of A and β_i is defined by $|b\rangle = \sum_i \beta_i |u_i\rangle$. The last qubit $|0\rangle$ is an ancilla, which will be used at the next stage. For the case of Eq. (4.1) we should choose $t = 2\pi/4$ and

$$\begin{aligned} \lambda_1 = 1 &= (0 \ 1)_2 & |u_1\rangle &= \frac{1}{\sqrt{2}} (|0\rangle - |1\rangle) \\ \lambda_2 = 2 &= (1 \ 0)_2 & |u_2\rangle &= \frac{1}{\sqrt{2}} (|0\rangle + |1\rangle) \\ \beta_1 &= \frac{1}{\sqrt{2}}(b_0 - b_1) & \beta_2 &= \frac{1}{\sqrt{2}}(b_0 + b_1). \end{aligned} \quad (4.3)$$

Thus, if the QPE stage is perfectly implemented in quantum computer, the quantum state $|\psi_1\rangle$ reduces to

$$|\psi_1\rangle = \frac{1}{2} \left[(b_0 - b_1) |01\rangle \otimes (|0\rangle - |1\rangle) + (b_0 + b_1) |10\rangle \otimes (|0\rangle + |1\rangle) \right] \otimes |0\rangle. \quad (4.4)$$

In $R(\lambda^{-1})$ -rotation stage we implement the controlled rotations to the ancilla qubit, whose angles are proportional to λ_i^{-1} . Using $\sin \theta \approx \theta$, the quantum state becomes approximately

$$|\psi_2\rangle \approx \sum_i \beta_i |\lambda_i\rangle |u_i\rangle \otimes \left[\sqrt{1 - \frac{C^2}{\lambda_i^2}} |0\rangle + \frac{C}{\lambda_i} |1\rangle \right] \quad (4.5)$$

after this stage, where C is some appropriate nonzero constant. For the case of Eq. (4.1) C is chosen as $C = (\sin \pi/4 + 2 \sin \pi/8)/2 \approx 0.736$. If, therefore, this stage is perfectly implemented, after this stage $|\psi_2\rangle$ becomes approximately

$$|\psi_2\rangle \approx \frac{1}{2} \left[(b_0 - b_1) |01\rangle \otimes (|0\rangle - |1\rangle) + (b_0 + b_1) |10\rangle \otimes (|0\rangle + |1\rangle) \right] \otimes \left[\sqrt{1 - \frac{C^2}{\lambda_i^2}} |0\rangle + \frac{C}{\lambda_i} |1\rangle \right]. \quad (4.6)$$

At the QPE[†] stage we undo the QPE implementation to uncompute the $|\lambda_i\rangle$. As a result, after this stage $|\lambda_i\rangle$ in Eq. (4.5) is changed into $|0\rangle^{\otimes n}$, which gives

$$|\psi_3\rangle = |0\rangle^{\otimes n} \otimes \sum_i \beta_i |u_i\rangle \otimes \left[\sqrt{1 - \frac{C^2}{\lambda_i^2}} |0\rangle + \frac{C}{\lambda_i} |1\rangle \right]. \quad (4.7)$$

For the case of Eq. (4.1) $|\psi_3\rangle$ reduces to

$$\begin{aligned} |\psi_3\rangle = |00\rangle \otimes & \left[\frac{1}{2} \left\{ (b_0 - b_1) \sqrt{1 - C^2} + (b_0 + b_1) \sqrt{1 - \frac{C^2}{4}} \right\} |00\rangle \right. \\ & + \frac{1}{2} \left\{ -(b_0 - b_1) \sqrt{1 - C^2} + (b_0 + b_1) \sqrt{1 - \frac{C^2}{4}} \right\} |10\rangle \\ & \left. + C(x_0|0\rangle + x_1|1\rangle) \otimes |1\rangle \right] \end{aligned} \quad (4.8)$$

where

$$\mathbf{x} = A^{-1} \mathbf{b} = \frac{1}{4} \begin{pmatrix} 3b_0 - b_1 \\ -b_0 + 3b_1 \end{pmatrix} \equiv \begin{pmatrix} x_0 \\ x_1 \end{pmatrix}. \quad (4.9)$$

Therefore, measuring the ancilla qubit, one can compute $A^{-1} \mathbf{b}$ if the measurement outcome is 1.

V. TRIPARTITE ENTANGLEMENT IN HHL ALGORITHM

In this section we discuss how much the HHL algorithm utilizes the entanglement efficiently as we discussed previously in the Grover's algorithm. In this reason we will compute the entanglement at each stage of the HHL algorithm. For simplicity, we will consider only the case of Eq. (4.1). Thus, the three-tangle[21] and π -tangle[39] will be computed explicitly after taking a partial trace over the ancilla qubit in Eqs. (4.4), (4.6), and (4.8).

Since the ancilla qubit is decoupled in $|\psi_1\rangle$ of Eq. (4.4), the first three-qubit state after the QPE stage is simply

$$|\bar{\psi}_1\rangle = \frac{1}{2} \left[(b_0 - b_1) |01\rangle \otimes (|0\rangle - |1\rangle) + (b_0 + b_1) |10\rangle \otimes (|0\rangle + |1\rangle) \right]. \quad (5.1)$$

From Eq. (4.6) one can compute $\bar{\rho}_2 = \text{Tr}_{\text{ancilla}} |\psi_2\rangle \langle \psi_2|$. It turns out that $\bar{\rho}_2$ is rank-2 mixed state and its spectral decomposition is

$$\bar{\rho}_2 = p |\phi_1\rangle \langle \phi_1| + (1 - p) |\phi_2\rangle \langle \phi_2| \quad (5.2)$$

where

$$p = \frac{1}{2} \left[1 + \sqrt{1 - 4\beta_1^2 \beta_2^2 (1 - \gamma^2)} \right] \quad \gamma = \sqrt{(1 - C^2) \left(1 - \frac{C^2}{4} \right)} + \frac{C^2}{2}. \quad (5.3)$$

In Eq. (5.2) $|\phi_1\rangle$ and $|\phi_2\rangle$ are the same with Eq. (3.2) if

$$x_1 = \frac{a_1}{\sqrt{a_1^2 + a_2^2}} \quad x_2 = \frac{a_2}{\sqrt{a_1^2 + a_2^2}} \quad (5.4)$$

where

$$\begin{aligned} a_1 &= \beta_1 \left[1 + \sqrt{1 - 4\beta_1^2 \beta_2^2 (1 - \gamma^2)} - 2\beta_2^2 (1 - \gamma^2) \right] \\ a_2 &= \beta_2 \gamma \left[1 + \sqrt{1 - 4\beta_1^2 \beta_2^2 (1 - \gamma^2)} \right]. \end{aligned} \quad (5.5)$$

Similarly, $\bar{\rho}_3 = \text{Tr}_{\text{ancilla}} |\psi_3\rangle\langle\psi_3|$ can be computed by making use of Eq. (4.8), whose spectral decomposition is

$$\bar{\rho}_3 = q |\varphi_1\rangle\langle\varphi_1| + (1 - q) |\varphi_2\rangle\langle\varphi_2| \quad (5.6)$$

where

$$q = \frac{1}{2} \left[1 + \sqrt{1 - 4(AC_2 - BC_1)^2} \right] \quad (5.7)$$

with

$$\begin{aligned} A &= \frac{1}{2} \left[(b_0 - b_1) \sqrt{1 - C^2} + (b_0 + b_1) \sqrt{1 - \frac{C^2}{4}} \right] \\ B &= \frac{1}{2} \left[-(b_0 - b_1) \sqrt{1 - C^2} + (b_0 + b_1) \sqrt{1 - \frac{C^2}{4}} \right] \\ C_1 &= C \frac{3b_0 - b_1}{4} \quad C_2 = C \frac{-b_0 + 3b_1}{4}. \end{aligned} \quad (5.8)$$

One can show $A^2 + B^2 + C_1^2 + C_2^2 = b_0^2 + b_1^2 = 1$ explicitly. In Eq. (5.6) $|\varphi_1\rangle$ and $|\varphi_2\rangle$ are

$$|\varphi_1\rangle = |00\rangle \otimes (y_1|0\rangle + y_2|1\rangle) \quad |\varphi_2\rangle = |00\rangle \otimes (-y_2|0\rangle + y_1|1\rangle) \quad (5.9)$$

where

$$y_1 = \frac{f_1}{\sqrt{f_1^2 + f_2^2}} \quad y_2 = \frac{f_2}{\sqrt{f_1^2 + f_2^2}} \quad (5.10)$$

with

$$f_1 = A^2 - B^2 + C_1^2 - C_2^2 + \sqrt{1 - 4(AC_2 - BC_1)^2} \quad f_2 = 2(AB + C_1 C_2). \quad (5.11)$$

A. Three-tangle

Using Ref. [21] it is easy to compute the three-tangle of $|\bar{\psi}_1\rangle$:

$$\tau_3(\bar{\psi}_1) = 4\beta_1^2\beta_2^2 = (b_0^2 - b_1^2)^2. \quad (5.12)$$

From Eq. (3.9) p_{\pm} for $\bar{\rho}_2$ is

$$p_{\pm} = \frac{a_{\pm}^2}{a_1^2 + a_2^2} \quad (5.13)$$

where $a_+^2 = \max(a_1^2, a_2^2)$ and $a_-^2 = \min(a_1^2, a_2^2)$. Thus, making use of Eq. (3.10) one can compute the three-tangle of $\bar{\rho}_2$, whose explicit expression is

$$\tau_3(\bar{\rho}_2) = \begin{cases} g(p) & p \leq p_- \text{ or } p \geq p_+ \\ 0 & p_- \leq p \leq p_+. \end{cases} \quad (5.14)$$

where $g(p) = \min[g_+(p), g_-(p)]$ with

$$g_{\pm}(p) = \frac{4}{(a_1^2 + a_2^2)^2} \left[(2p - 1)a_1a_2 \pm \sqrt{p(1-p)}(a_1^2 - a_2^2) \right]^2. \quad (5.15)$$

Of course, p , a_1 , and a_2 are given in Eqs. (5.3) and (5.5). Since $|\varphi_1\rangle$ and $|\varphi_2\rangle$ are fully separable states, the three-tangle of $\bar{\rho}_3$ is

$$\tau_3(\bar{\rho}_3) = 0. \quad (5.16)$$

The three-tangles for $|\bar{\psi}_1\rangle$, $\bar{\rho}_2$, and $\bar{\rho}_3$ are plotted in Fig. 4(a) as a function of b_0^2 . The black solid, red dashed, and blue dotted lines correspond to $\tau_3(\bar{\psi}_1)$, $\tau_3(\bar{\rho}_2)$, and $\tau_3(\bar{\rho}_3)$. From this figure we understand that the QPE stage generates the three-tangle represented by the black solid line. This three-tangle reduces to red dashed line in the $R(\lambda^{-1})$ -rotation stage. Finally, the matrix inversion task is accomplished in the QPE[†] stage at the price of complete annihilation of the three-tangle.

B. π -tangle

The π -tangle is a global negativity[40]-based tripartite entanglement measure[39]. While three-tangle cannot detect the tripartite entanglement of the W-state class, π -tangle can detect it. For a three-qubit state ρ the global negativities are given by

$$\mathcal{N}^A = \|\rho^{TA}\| - 1, \quad \mathcal{N}^B = \|\rho^{TB}\| - 1, \quad \mathcal{N}^C = \|\rho^{TC}\| - 1, \quad (5.17)$$

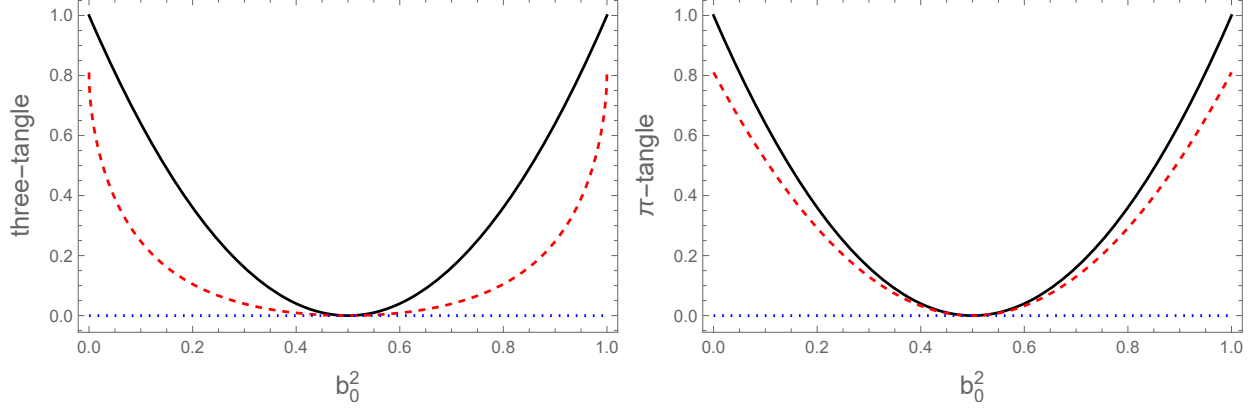


FIG. 4: (Color online) (a) Plot of the three-tangles as a function of b_0^2 . The black solid, red dashed, and blue dotted lines correspond to $\tau_3(\bar{\psi}_1)$, $\tau_3(\bar{\rho}_2)$, and $\tau_3(\bar{\rho}_3)$. (b) Plot of the π -tangles as a function of b_0^2 . The black solid, red dashed, and blue dotted lines correspond to $\pi_3(\bar{\psi}_1)$, $\pi_3(\bar{\rho}_2)$, and $\pi_3(\bar{\rho}_3)$.

where $||R|| = \text{Tr}\sqrt{RR^\dagger}$, and the superscripts T_A , T_B and T_C represent the partial transposes of ρ with respect to the qubits A , B and C respectively. Using the separability criterion based on partial transpose [41–43], it is easy to show that the global negativities vanish for separable states. It is worthwhile noting that the computation of the global negativities is relatively simple compared to the concurrence or three-tangle for mixed states since it does not need the convex-roof extension defined in Eq. (3.4). In addition, the negativities also satisfy the monogamy inequality

$$\mathcal{N}_{AB}^2 + \mathcal{N}_{AC}^2 \leq \mathcal{N}_{A(BC)}^2 \quad (5.18)$$

like concurrence. Then, the π -tangle is defined as

$$\pi_{ABC} = \frac{1}{3}(\pi_A + \pi_B + \pi_C), \quad (5.19)$$

where

$$\pi_A = \mathcal{N}_{A(BC)}^2 - (\mathcal{N}_{AB}^2 + \mathcal{N}_{AC}^2) \quad \pi_B = \mathcal{N}_{B(AC)}^2 - (\mathcal{N}_{AB}^2 + \mathcal{N}_{BC}^2) \quad \pi_C = \mathcal{N}_{(AB)C}^2 - (\mathcal{N}_{AC}^2 + \mathcal{N}_{BC}^2). \quad (5.20)$$

It is easy to show that the π -tangles for $|GHZ\rangle$ and $|W\rangle$ become

$$\pi_{ABC}(|GHZ\rangle) = 1 \quad \pi_{ABC}(|W\rangle) = \frac{4}{9}(\sqrt{5} - 1) \sim 0.55 \quad (5.21)$$

where

$$|GHZ\rangle = \frac{1}{\sqrt{2}}(|000\rangle + |111\rangle) \quad |W\rangle = \frac{1}{\sqrt{3}}(|001\rangle + |010\rangle + |100\rangle). \quad (5.22)$$

Thus, the π -tangle detects W-like(as well as GHZ-like) entanglement.

It is straightforward to compute the π -tangle of $|\bar{\psi}_1\rangle$, $\bar{\rho}_2$, and $\bar{\rho}_3$. The final result is

$$\pi_3(\bar{\psi}_1) = 4\beta_1^2\beta_2^2 = (b_0^2 - b_1^2)^2 \quad \pi_3(\bar{\rho}_2) = \frac{4a_1^2a_2^2}{(a_1^2 + a_2^2)^2}(2p - 1)^2 \quad \pi_3(\bar{\rho}_3) = 0. \quad (5.23)$$

This is plotted in Fig. 4(b) as a function of b_0^2 . The black solid, red dashed, and blue dotted lines correspond to $\pi_3(\bar{\psi}_1)$, $\pi_3(\bar{\rho}_2)$, and $\pi_3(\bar{\rho}_3)$. The behavior of the π -tangle is similar to that of the three-tangle. The only difference is that $\pi_3(\bar{\psi}_1) - \pi_3(\bar{\rho}_2)$ is generally smaller than $\tau_3(\bar{\psi}_1) - \tau_3(\bar{\rho}_2)$. This means that the decrease of π -tangle in the $R(\lambda^{-1})$ -rotation stage is smaller compared to the three-tangle.

VI. CONCLUSION

In this paper we examine a question ‘how much the HHL algorithm exploits the quantum entanglement efficiently?’. In this reason we computed the tripartite entanglement explicitly at the every steps of the HHL algorithm by choosing the explicit example (4.1).

As Fig. 4 shows, the three-tangle and π -tangle exhibit similar behavior. At the QPE stage the tripartite entanglement is generated. The amount of it is dependent on b_0^2 . If $b_0^2 = 0$ or 1, maximal tripartite entanglement is generated at this stage. For other case partial entanglement is generated. At the $R(\lambda^{-1})$ -rotation stage some entanglement is used. Thus, the net tripartite entanglement is reduced. At the final QPE[†] stage the matrix inversion task is completed at the price of vanishing all entanglement.

The HHL algorithm is known as an optimal[16] in the matrix inversion task. It is also known that entanglement is a physical resource in quantum information processing. Then, the following question arises: why maximal creation of entanglement and complete annihilation of it do not occur? As discussed in Sec. II similar phenomenon happens in the Grover’s algorithm for large N even though it is known to be optimal[28] in the quantum searching task. This means that from an aspect of entanglement, both algorithms do not use entanglement efficiently to some extent. We think there are additional quantities as well as entanglement, which may play important role in the quantum algorithm. Similar situation

happens in the quantum illumination[44–46]. In this case the quantum discord is known to be important[47, 48].

Even though we have not presented explicitly in the paper, one can show that all bipartite entanglement of $|\bar{\psi}_1\rangle$, $\bar{\rho}_2$, and $\bar{\rho}_3$ are zero. This means that $|\bar{\psi}_1\rangle$ and $\bar{\rho}_2$ are in the GHZ-class[29]. We do not exactly understand why the W-type entanglement does not arise. All the questions will be discussed in the future.

-
- [1] M. A. Nielsen and I. L. Chuang, *Quantum Computation and Quantum Information* (Cambridge University Press, Cambridge, England, 2000).
 - [2] E. Schrödinger, *Die gegenwärtige Situation in der Quantenmechanik*, *Naturwissenschaften*, **23** (1935) 807.
 - [3] R. Horodecki, P. Horodecki, M. Horodecki, and K. Horodecki, *Quantum Entanglement*, *Rev. Mod. Phys.* **81** (2009) 865 [quant-ph/0702225] and references therein.
 - [4] C. H. Bennett, G. Brassard, C. Crepeau, R. Jozsa, A. Peres and W. K. Wootters, *Teleporting an Unknown Quantum State via Dual Classical and Einstein-Podolsky-Rosen Channels*, *Phys.Rev. Lett.* **70** (1993) 1895.
 - [5] Y. H. Luo et al., *Quantum Teleportation in High Dimensions*, *Phys. Rev. Lett.* **123** (2019) 070505 [arXiv:1906.09697 (quant-ph)].
 - [6] C. H. Bennett and S. J. Wiesner, *Communication via one- and two-particle operators on Einstein-Podolsky-Rosen states*, *Phys. Rev. Lett.* **69** (1992) 2881.
 - [7] V. Scarani, S. Lblisdir, N. Gisin and A. Acin, *Quantum cloning*, *Rev. Mod. Phys.* **77** (2005) 1225 [quant-ph/0511088] and references therein.
 - [8] A. K. Ekert, *Quantum Cryptography Based on Bell’s Theorem*, *Phys. Rev. Lett.* **67** (1991) 661.
 - [9] C. Kollmitzer and M. Pivk, *Applied Quantum Cryptography* (Springer, Heidelberg, Germany, 2010).
 - [10] K. Wang, X. Wang, X. Zhan, Z. Bian, J. Li, B. C. Sanders, and P. Xue, *Entanglement-enhanced quantum metrology in a noisy environment*, *Phys. Rev.* **A97** (2018) 042112 [arXiv:1707.08790 (quant-ph)].
 - [11] T. D. Ladd, F. Jelezko, R. Laflamme, Y. Nakamura, C. Monroe, and J. L. O’Brien, *Quantum*

- Computers*, Nature, **464** (2010) 45 [arXiv:1009.2267 (quant-ph)].
- [12] G. Vidal, *Efficient classical simulation of slightly entangled quantum computations*, Phys. Rev. Lett. **91** (2003) 147902 [quant-ph/0301063].
 - [13] F. Arute et al., Quantum supremacy using a programmable superconducting processor, Nature **574** (2019) 505. Its supplementary information is given in arXiv:1910.11333.
 - [14] P. W. Shor, *Algorithms for Quantum Computation: Discrete Logarithms and Factoring*, Proc. 35th Annual Symposium on Foundations of Computer Science (1994) 124.
 - [15] L. K. Grover, *A fast quantum mechanical algorithm for database search*, Proc. 28th Annual ACM Symposium on the Theory of Computing (1996) 212 [quant-ph/9605043].
 - [16] A. W. Harrow, A. Hassidim, and S. Lloyd, *Quantum algorithm for solving linear systems of equations*, Phys. Rev. Lett. **15** (2009) 150502 [arXiv:0811.3171 (quant-ph)].
 - [17] D. W. Berry, G. Ahokas, R. Cleve, and B. C. Sanders, *Efficient quantum algorithms for simulating sparse Hamiltonians*, Comm. Math. Phys. **270** (2007) 359 [arXiv:quant-ph/0508139 (quant-ph)].
 - [18] L. Wossnig, Z. Zhao, and A. Prakash, *A quantum linear system algorithm for dense matrices*, Phys. Rev. Lett. **120** (2018) 050502 [arXiv:1704.06174 (quant-ph)].
 - [19] Y. Lee, J. Joo, and S. Lee, *Hybrid quantum linear equation algorithm and its experimental test on IBM Quantum Experience*, Scientific Reports **9** (2019) 4778 [arXiv:1807.10651 (quant-ph)].
 - [20] J. Pan, Y. Cao, X. Yao, Z. Li, C. Ju, X. Peng, S. Kais, and J. Du, *Experimental realization of quantum algorithm for solving linear systems of equations*, Phys. Rev. **A 89** (2014) 022313 [arXiv:1302.1946 (quant-ph)].
 - [21] V. Coffman, J. Kundu and W. K. Wootters, *Distributed entanglement*, Phys. Rev. **A61** (2000) 052306 [quant-ph/9907047].
 - [22] L. K. Grover, *Quantum Mechanics helps in searching for a needle in a haystack*, Phys. Rev. Lett. **79** (1997) 325 [quant-ph/9706033].
 - [23] C. H. Bennett, E. Bernstein, G. Brassard, and U. Vazirani, *Strengths and Weaknesses of Quantum Computing*, SIAM Journal on Computing, **26** (1997) 1510 [quant-ph/9701001].
 - [24] M. Boyer, G. Brassard, P. Hoeyer, and A. Tapp, *Tight bounds on quantum searching*, Fortschritte der Physik, **46** (1998) 493 [quant-ph/9605034].
 - [25] L. K. Grover, *How fast can a quantum computer search?*, quant-ph/9809029.
 - [26] S. Hill and W. K. Wootters, *Entanglement of a Pair of Quantum Bits*, Phys. Rev. Lett. **78**

- (1997) 5022 [quant-ph/9703041].
- [27] W. K. Wootters, *Entanglement of Formation of an Arbitrary State of Two Qubits*, Phys. Rev. Lett. **80** (1998) 2245 [quant-ph/9709029].
 - [28] C. Zalka, *Grover's quantum searching algorithm is optimal*, Phys. Rev. **A 60** (1999) 2746 [quant-ph/9711070].
 - [29] W. Dür, G. Vidal, and J. I. Cirac, *Three qubits can be entangled in two inequivalent ways*, Phys. Rev. **A62** (2000) 062314 [quant-ph/0005115].
 - [30] C. H. Bennett, D. P. DiVincenzo, J. A. Smolin and W. K. Wootters, *Mixed-state entanglement and quantum error correction*, Phys. Rev. **A54** (1996) 3824 [quant-ph/9604024].
 - [31] A. Uhlmann, *Fidelity and concurrence of conjugate states*, Phys. Rev. **A 62** (2000) 032307 [quant-ph/9909060].
 - [32] R. Lohmayer, A. Osterloh, J. Siewert and A. Uhlmann, *Entangled Three-Qubit States without Concurrence and Three-Tangle*, Phys. Rev. Lett. **97** (2006) 260502 [quant-ph/0606071].
 - [33] A. Osterloh, J. Siewert, and A. Uhlmann, *Tangles of superpositions and the convex-roof extension*, Phys. Rev. **A 77** (2008) 032310 [arXiv:0710.5909 (quant-ph)].
 - [34] E. Jung, M. R. Hwang, D. K. Park and J. W. Son, *Three-tangle for Rank-3 Mixed States: Mixture of Greenberger-Horne-Zeilinger, W and flipped W states*, Phys. Rev. **A79** (2009) 024306, arXiv:0810.5403 (quant-ph).
 - [35] E. Jung, M. R. Hwang, D. K. Park, and S. Tamaryan, *Three-Party Entanglement in Tripartite Teleportation Scheme through Noisy Channels*, Quant. Inf. Comp. **40** (2010) 0377 [arXiv:0904.2807 (quant-ph)].
 - [36] R. Cleve, A. Ekert, C. Macchiavello, and M. Mosca, *Quantum Algorithms Revisited*, quant-ph/9708016.
 - [37] A. Luis and J. Peřina, *Optimum phase-shift estimation and the quantum description of the phase difference*, Phys. Rev. **A 54** (1996) 4564.
 - [38] see also <https://qiskit.org/textbook/ch-algorithms/quantum-phase-estimation.html>.
 - [39] Y. U. Ou and H. Fan, *Monogamy Inequality in terms of Negativity for Three-Qubit States*, Phys. Rev. **A75** (2007) 062308 [quant-ph/0702127].
 - [40] G. Vidal and R. F. Werner, *Computable measure of entanglement*, Phys. Rev. **A65** (2002) 032314 [quant-ph/0102117].
 - [41] A. Peres, *Separability Criterion for Density Matrices*, Phys. Rev. Lett. **77** (1996) 1413 [quant-

- ph/9604005].
- [42] M. Horodecki, P. Horodecki and R. Horodecki, *Separability of mixed states: necessary and sufficient conditions*, Phys. Lett. **A 223** (1996) 1 [quant-ph/9605038].
 - [43] P. Horodecki, *Separability criterion and inseparable mixed states with partial transposition*, Phys. Lett. **A 232** (1997) 333 [quant-ph/9703004].
 - [44] S. Lloyd, *Enhanced Sensitivity of Photodetection via Quantum Illumination*, Science, **321**, 1463 (2008).
 - [45] S.-H. Tan, B. I. Erkmen, V. Giovannetti, S. Guha, S. Lloyd, L. Maccone, S. Pirandola, and J. H. Shapiro, *Quantum Illumination with Gaussian States*, Phys. Rev. Lett. **101**, 253601 (2008) [arXiv:0810.0534 (quant-ph)].
 - [46] E. Jung and D. K. Park, *Quantum Illumination with three-mode Gaussian State*, Quant. Inf. Proc. **21** (2022) 71 [arXiv:2107.05203 (quant-ph)].
 - [47] C. Weedbrook, S. Pirandola, J. Thompson, V. Vedral, and M. Gu, *How discord underlies the noise resilience of quantum illumination*, New J. Phys. **18** (2016) 043027.
 - [48] M. Bradshaw, S. M. Assad, J. Y. Haw, S. H. Tan, P. K. Lam, M. Gu, *Overarching framework between Gaussian quantum discord and Gaussian quantum illumination*, Phys. Rev. **A 95** (2017) 022333 [arXiv:1611.10020 (quant-ph)].
 - [49] see also <https://qiskit.org/textbook/ch-algorithms/quantum-fourier-transform.html>.

Appendix A: Quantum Phase Estimation (QPE)

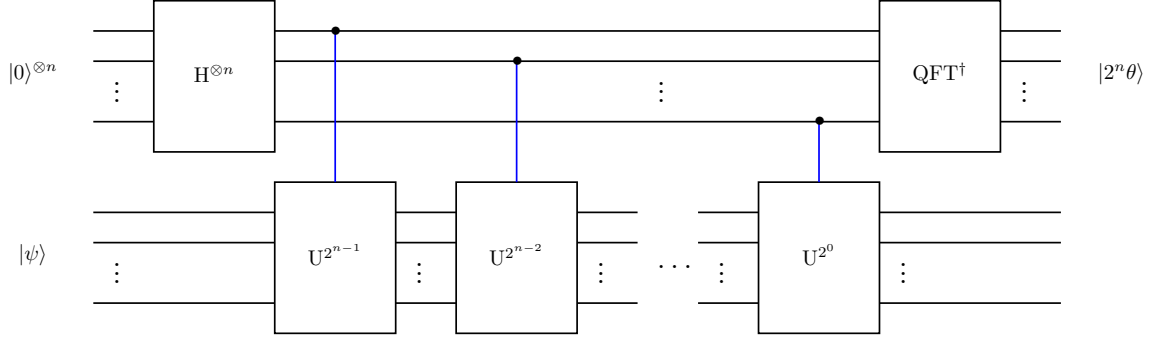


FIG. 5: (Color online) The quantum circuit of QPE. In the figure QFT means quantum Fourier transform. If $|\psi\rangle$ is an eigenvector of the unitary operator U in a form $U|\psi\rangle = e^{2\pi i\theta}|\psi\rangle$, this QPE quantum circuit generates $|2^n\theta\rangle$ in the c-register.

In this appendix QPE will be discussed in detail and Eq. (4.2) will be derived explicitly. The quantum circuit of QPE[38] is plotted in Fig. 5. In Fig. 5 QFT stands for quantum Fourier transform[1, 14, 49], which is defined by the unitary operator U_{QFT} obeying

$$|\tilde{x}\rangle = U_{QFT}|x\rangle = \frac{1}{\sqrt{N}} \sum_{y=0}^{N-1} e^{\frac{2\pi i x \cdot y}{N}} |y\rangle \quad (\text{A.1})$$

where $|x\rangle$ is arbitrary n -qubit state and $N = 2^n$. As Fig. 5 shows, QPE consists of two registers. First register starts with $|0\rangle^{\otimes n}$, which we will call ‘c-register’. Second register starts with some quantum state $|\psi\rangle$, which we will call ‘t-register’. In the figure U is a certain unitary operator. If $|\psi\rangle$ is an eigenvector of U in a form

$$U|\psi\rangle = e^{2\pi i\theta}|\psi\rangle, \quad (\text{A.2})$$

the quantum circuit in Fig. 5 generates $|2^n\theta\rangle \otimes |\psi\rangle$ in the c-register and t-register respectively at the final stage. If the whole process of QPE is represented by an unitary operator U_{QPE} , this fact implies

$$U_{QPE} \left[|0\rangle^{\otimes n} \otimes |\psi\rangle \right] = |2^n\theta\rangle \otimes |\psi\rangle. \quad (\text{A.3})$$

Thus, measuring the c-register at the final step, one can estimate the phase θ . For example, if the outcome is m , one can conjecture $\theta = m/2^n$.⁴

Now, let us consider the case that $|\psi\rangle$ is not an eigenvector of U . Let the eigenvectors of U be $|u_j\rangle$ obeying

$$U|u_j\rangle = e^{2\pi i\theta_j}|u_j\rangle. \quad (\text{A.4})$$

Since a set $\{|u_j\rangle\}$ is a complete, $|\psi\rangle$ can be expressed as a linear combination of $|u_j\rangle$ in a form

$$|\psi\rangle = \sum_j \beta_j |u_j\rangle. \quad (\text{A.5})$$

Using a fact that U_{QPE} is a linear operator, it is straightforward to show

$$U_{QPE} \left[|0\rangle^{\otimes n} \otimes |\psi\rangle \right] = \sum_j \beta_j |2^n \theta_j\rangle \otimes |u_j\rangle \quad (\text{A.6})$$

in this case.

Since $U = e^{iAt}$ and $|\psi\rangle = |b\rangle$ in the HHL algorithm and they obey

$$A|u_j\rangle = \lambda_j |u_j\rangle \quad |b\rangle = \sum_j \beta_j |u_j\rangle, \quad (\text{A.7})$$

the final state after QPE becomes

$$|\psi_{final}\rangle = \sum_j \beta_j |2^n \frac{\lambda_j}{2\pi} t\rangle \otimes |u_j\rangle. \quad (\text{A.8})$$

Thus, if t is chosen as $t = 2\pi/2^n$, one can derive Eq. (4.2).

⁴ If θ is not a form of $m/2^n$, the quantum circuit produces an inequality $\theta_{min} < \theta < \theta_{max}$, where $\theta_{max} - \theta_{min}$ decreases with increasing n .